Journal of Scientific Computing, Vol. 16, No. 1, March 2001 (© 2001)

Outflow Boundary Conditions for the Fourier Transformed One-Dimensional Vlasov–Poisson System

Bengt Eliasson[1]

Received December 18, 2000; accepted (in revised form) March 5, 2001

In order to facilitate numerical simulations of plasma phenomena where kinetic processes are important, we have studied the technique of Fourier transforming the Vlasov equation analytically in the velocity space, and solving the resulting equation numerically. Special attention has been paid to the boundary conditions of the Fourier transformed system. By using outgoing wave boundary conditions in the Fourier transformed space, small-scale information in velocity space is carried outside the computational domain and is lost. Thereby the so-called recurrence phenomenon is reduced. This method is an alternative to using numerical dissipation or smoothing operators in velocity space. Different high-order methods are used for computing derivatives as well as for the time-stepping, leading to an over-all fourth-order method.

KEY WORDS: Vlasov equation; Fourier method; Outflow boundary.

1. INTRODUCTION

Methods of solving numerically the Vlasov equation have been developed for many decades, including methods based on Hermite and Fourier expansions [1, 3] and methods based on the convective structure of the Vlasov equation [2]. Convective schemes have also been developed for the collisional Boltzmann equation [4].

A problem with the Vlasov equation is its tendency of structuring in velocity space (due to free streaming terms), in which steep gradients are created and problems of calculating the v (velocity) derivative of the function accurately increase with time [1].

[1] Department of Scientific Computing, P.O. Box 120, SE-752 37 Uppsala, Sweden. Department of Astronomy and Space Physics, Box 515, SE-751 21 Uppsala, Sweden. E-mail: be@tdb.uu.se, be@irfu.se

0885-7474/01/0300-0001$19.50/0

Due to the sampling (Nyqvist) theorem, the tendency of structuring of the Vlasov equation makes it impossible to represent all pats of the solution of a uniform grid after a finite time. If not treated carefully, this problem may eventually lead to the so-called *recurrence phenomenon* where parts of the initial condition artificially re-appear on the numerical grid [2].

In applications, the recurrence phenomenon may in some cases be unimportant if other processes dominate [7], but can be important if, for example, the long-time behaviour of a single wave is studied [8].

One method of minimising effects due to the recurrence phenomenon is to have a dense enough grid, so that the interesting physical results have the time to develop, and then to stop the simulation before the recurrence phenomenon takes place [8]. Another method is to apply smoothing operators to the numerical solution so that the finest structures never appear on the numerical grid [2].

The method used in the present paper is related to the second of the above two methods, but instead of direct damping of small-scale information, the small-scale information in velocity space is removed through an outgoing wave boundary condition in the Fourier transformed velocity space. The position of the boundary in the Fourier transformed variable determines the amount of small-scale information saved in velocity space. The objective of the method is thus not to resolve the solution fully but only to a certain degree, and to remove the finest structures of the solution. How much of the small-scale information one needs to save strongly depends on the physical problem.

In Section 2.1 the three-dimensional Vlasov–Maxwell system is discussed, together with the Fourier transform technique in velocity space. In Sections 2.2–2.5 the one-dimensional Vlasov–Poisson system is discussed, and well-posed boundary conditions are derived in preparation for the numerical simulation of the Fourier-transformed system. In Section 3 the numerical schemes used to approximate the time-dependent solution of the Vlasov–Poisson system are described. In Section 4 numerical experiments are presented and compared with known theory and with simulations with other methods. In Section 5 some conclusions are drawn regarding the usefulness of the method.

2. THE VLASOV–MAXWELL SYSTEM

2.1. The Three-Dimensional System

The Vlasov equation

$$\frac{\partial f_\alpha}{\partial t} + \mathbf{v} \cdot \nabla_x f_\alpha + \frac{q_\alpha}{m_\alpha} (\mathbf{E} + \mathbf{v} \times \mathbf{B}) \cdot \nabla_v f_\alpha = 0 \tag{1}$$

describes the action of the electromagnetic field on charged particles of type α (e.g., "electrons" or "singly ionised oxygen ions"), each particle having the electric charge q_α and mass m_α. One equation is needed for each species of particles.

The charge and current densities act as sources of self-consistent electromagnetic fields according to the Maxwell equations

$$\nabla \cdot \mathbf{E} = \frac{1}{\varepsilon_0} \sum_\alpha q_\alpha n_\alpha \tag{2}$$

$$\nabla \cdot \mathbf{B} = 0 \tag{3}$$

$$\nabla \times \mathbf{E} = -\frac{\partial \mathbf{B}}{\partial t} \tag{4}$$

$$\nabla \times \mathbf{B} = \mu_0 \sum_\alpha q_\alpha n_\alpha \mathbf{v}_\alpha + \varepsilon_0 \mu \frac{\partial \mathbf{E}}{\partial t} \tag{5}$$

where the particle number densities n_α and mean velocities $\mathbf{v}_\alpha$ are obtained as moments of the distribution function, as

$$n_\alpha(\mathbf{x}, t) = \int_{-\infty}^{\infty} f_\alpha(\mathbf{x}, \mathbf{v}, t)\, \mathrm{d}^3 v \tag{6}$$

and

$$\mathbf{v}_\alpha(\mathbf{x}, t) = \frac{1}{n_\alpha(\mathbf{x}, t)} \int_{-\infty}^{\infty} \mathbf{v} f_\alpha(\mathbf{x}, \mathbf{v}, t)\, \mathrm{d}^3 v \tag{7}$$

respectively. The Vlasov equations together with the Maxwell equations form a closed system.

By using the Fourier transform pair

$$f_\alpha(\mathbf{x}, \mathbf{v}, t) = \int_{-\infty}^{\infty} \hat{f}_\alpha(\mathbf{x}, \eta, t)\, e^{-\mathrm{i}\eta \cdot \mathbf{v}}\, d^3\eta \tag{8}$$

$$\hat{f}_\alpha(\mathbf{x}, \eta, t) = \frac{1}{(2\pi)^3} \int_{-\infty}^{\infty} f_\alpha(\mathbf{x}, \mathbf{v}, t)\, e^{\mathrm{i}\eta \cdot \mathbf{v}}\, \mathrm{d}^3\eta \tag{9}$$

the velocity variable $\mathbf{v}$ is transformed into a new variable η and the unknown function $f(\mathbf{x}, \mathbf{v}, t)$ is changed to a new, complex valued, function $\hat{f}(\mathbf{x}, \eta, t)$, which obeys the transformed Vlasov equation

$$\frac{\partial \hat{f}_\alpha}{\partial t} - \mathrm{i}\nabla_x \cdot \nabla_\eta \hat{f}_\alpha - \mathrm{i}\frac{q_\alpha}{m_\alpha} \{\mathbf{E} \cdot \eta \hat{f}_\alpha + \nabla_\eta \cdot [(\mathbf{B} \times \eta)\, \hat{f}_\alpha]\} = 0 \tag{10}$$

The nabla operators ∇_x and ∇_η denote differentiation with respect to $\mathbf{x}$ and η, respectively.

Equation (10) is again solved together with the Maxwell equations, where the particle number densities and mean velocities are obtained as

$$n_\alpha(\mathbf{x}, t) = (2\pi)^3 \hat{f}_\alpha(\mathbf{x}, \mathbf{0}, t) \tag{11}$$

and

$$\mathbf{v}_\alpha(\mathbf{x}, t) = -\mathrm{i} \frac{(2\pi)^3}{n_\alpha(\mathbf{x}, t)} [\nabla_\eta \hat{f}_\alpha(\mathbf{x}, \eta, t)]_{\eta = \mathbf{0}} \tag{12}$$

respectively. One can note that the integrals over infinite $\mathbf{v}$ space have been converted to evaluations at a single point in η space. The factor $(2\pi)^3$ in Eqs. (9), (11), and (12) is valid for three velocity dimensions. For two velocity dimensions the factor is $(2\pi)^2$ and in one dimension the factor is 2π.

2.2. The One-Dimensional Vlasov–Poisson System

In order to explore advantages and disadvantages of the Fourier transformation technique just described, we have chosen to study numerically a simpler case, the one-dimensional Vlasov–Poisson system consisting of electrons and ions, with the ions assumed fixed uniformly in space. These assumptions lead to the system

$$\begin{aligned} &\frac{\partial f}{\partial t} + v \frac{\partial f}{\partial x} - \frac{eE}{m} \frac{\partial f}{\partial v} = 0 \\ &\frac{\partial E(x, t)}{\partial x} = \frac{e}{\varepsilon_0} \left[n_0 - \int_{-\infty}^{\infty} f(x, v, t)\, \mathrm{d}v \right] \end{aligned} \tag{13}$$

where n_0 is the neutralising heavy ion density background.

By using the Fourier transform pair

$$f(x, v, t) = \int_{-\infty}^{\infty} \hat{f}(x, \eta, t)\, \mathrm{e}^{-\mathrm{i}\eta v}\, \mathrm{d}\eta \tag{14}$$

$$\hat{f}(x, \eta, t) = \frac{1}{2\pi} \int_{-\infty}^{\infty} f(x, v, t)\, e^{\mathrm{i}\eta v}\, \mathrm{d}v \tag{15}$$

Eq. (13) is transformed into

$$\frac{\partial \hat{f}}{\partial t} - \mathrm{i}\,\frac{\partial^2 \hat{f}}{\partial x\,\partial \eta} + \mathrm{i}\,\frac{eE}{m}\,\eta \hat{f} = 0$$
$$\frac{\partial E(x,t)}{\partial x} = \frac{e}{\varepsilon_0}\,[n_0 - 2\pi \hat{f}(x,0,t)] \tag{16}$$

Equation (16) has been studied analytically, by means of a similar Fourier transform technique as the one we use here, by H. Neunzert [9, 10].

The systems (13) and (16) can be cast into dimensionless form by a scaling of variables: the time t is scaled to the inverse of the plasma frequency $\omega_{\mathrm{p}}^{-1} = \sqrt{\varepsilon_0 m/(n_0 e^2)}$, the velocity v is scaled to the thermal velocity v_{th}; the new variable η is then scaled to the inverse of the thermal velocity, and the spatial variable x is scaled to the Debye length $r_{\mathrm{D}} = v_{\mathrm{th}}\omega_{\mathrm{p}}^{-1}$. Finally, the function $\hat{f}$ is scaled to the background density n_0, the function f is scaled to n_0/v_{th} and the electric field E is scaled to the quantity $v_{\mathrm{th}}\sqrt{n_0 m/\varepsilon_0}$. By this scaling of variables, the systems (13) and (16) attain the dimensionless form

$$\frac{\partial f}{\partial t} + v\,\frac{\partial f}{\partial x} - E\,\frac{\partial f}{\partial v} = 0 \tag{17}$$

$$\frac{\partial E(x,t)}{\partial x} = 1 - \int_{-\infty}^{\infty} f(x,v,t)\,\mathrm{d}v \tag{18}$$

and

$$\frac{\partial \hat{f}}{\partial t} - \mathrm{i}\,\frac{\partial^2 \hat{f}}{\partial x\,\partial \eta} + \mathrm{i}\eta E \hat{f} = 0 \tag{19}$$

$$\frac{\partial E(x,t)}{\partial x} = 1 - 2\pi \hat{f}(x,0,t) \tag{20}$$

respectively.

2.3. The Problem of Structuring in Velocity Space

This section contains a justification or motivation for solving numerically the Fourier transformed Vlasov–Poisson system in (x, η, t) space instead of the original system in (x, v, t) space.

Due to the property of conservation of phase memory, the Vlasov–Poisson system in phase (x, v, t) space may develop fine structures in velocity space, since no smearing of the solution occurs. This can be illustrated by a simple example:

Assume that the electric field is weak so that the Vlasov equation can be approximated by

$$\frac{\partial f}{\partial t} + v \frac{\partial f}{\partial x} = 0 \tag{21}$$

with the special choice of initial condition

$$f(x, v, 0) = f_0(x, v) = [1 + A \cos(k_x x)]\, e^{-v^2/2} \tag{22}$$

The solution to the initial value problem is

$$f(x, v, t) = f_0(x - vt, v) = [1 + A \cos(k_x x - k_x vt)]\, e^{-v^2/2} \tag{23}$$

This solution becomes more and more structured in the velocity direction with increasing time; it will in fact be impossible to store the solution after a finite time due to the Nyqvist theorem, that states that one needs at least two grid points per wavelength in order to represent a solution on an equidistant grid.

For this simple example it is possible to calculate the time after which the solution will be impossible to store: Assume that the grid size in v direction is Δv, and that function values are stored for $v = 0, \pm \Delta v, \pm 2\Delta v, ..., \pm N_v \Delta v$. The "wave-length" of the function $\cos(k_x x - k_x vt)$ is $\lambda_v = 2\pi/k_x t$ in the velocity direction. The Nyqvist theorem states the condition $\lambda_v/\Delta v > 2$ for storing the solution, which for the problem gives the condition $2\pi/k_x t\, \Delta v > 2$. This condition only holds for times $t < \pi/k_x \Delta v$. After this time it is impossible to represent the solution on the grid.

The recurrence effect [2] occurs at the time $T_c = 2\pi/k_x \Delta v$, which is the time for the values of the initial condition to re-appear on the numerical grid because of the Nyqvist theorem just described.

2.4. Some Properties of the Fourier Transformed System

In general $f(x, v, t)$ decreases as a Gaussian function $\sim \exp(-\alpha v^2)$ for large values of v. This behaviour guarantees that the inverse Fourier transformed function $\hat{f}(x, \eta, t)$ is a smooth function in η; it is an analytic function for all complex η and therefore all η-derivatives are well-defined. This is favourable when the η derivative in Eq. (19) is approximated by a numerical difference approximation.

The difference in behaviour for the Fourier transformed system compared to the original system can be illustrated by the example in the previous section; taking the Fourier transform of the solution (23) in the velocity space yields

$$\hat{f}(x, \eta, t) = \frac{1}{\sqrt{2\pi}} \left\{ e^{-\eta^2/2} + \frac{A}{2} [\cos(k_x x)(e^{-(\eta - k_x t)^2/2} + e^{-(\eta + k_x t)/2}) \right.$$
$$\left. + \mathrm{i} \sin(k_x x)(e^{-(\eta - k_x t)^2/2} - e^{-(\eta + k_x t)^2/2})] \right\} \tag{24}$$

This function does not become structured for large times. The $\exp[-(\eta - t)^2/2]$ and $\exp[-(\eta + t)^2/2]$ terms represent smooth wave packets moving away from the origin $\eta = 0$. Instead of becoming *structured*, the Fourier transformed solution becomes *wider* with increasing time.

Since the original distribution function $f(x, v, t)$ is real-valued the Fourier transformed function $\hat{f}(x, \eta, t)$ fulfils the relation

$$\hat{f}(x, -\eta, t) = [\hat{f}(x, \eta, t)]^* \tag{25}$$

where $*$ denotes complex conjugation. Therefore it is only necessary to solve the problem for positive η to obtain the solution for all η. For the derivatives one can easily show that the relation

$$\frac{\partial^n \hat{f}(x, -\eta, t)}{\partial \eta^n} = (-1)^n \left[\frac{\partial^n \hat{f}(x, \eta, t)}{\partial \eta^n} \right]^* \tag{26}$$

holds. Thus for even numbers of derivatives of the function $\hat{f}$ with respect to η, the real part is even and the imaginary part is odd with respect to η. For odd numbers of derivatives of $\hat{f}$, the opposite holds.

2.5. Invariants of the Vlasov–Poisson System

The one-dimensional system (17) with periodic boundary conditions describes a closed, undamped system and has several invariants with respect to time, such as

$$S = \int_0^L \int_{-\infty}^{\infty} f^2(x, v, t)\, \mathrm{d}v\, \mathrm{d}x \tag{27}$$

$$N = \int_0^L \int_{-\infty}^{\infty} f(x, v, t)\, \mathrm{d}v\, \mathrm{d}x \tag{28}$$

$$P = \int_0^L \int_{-\infty}^{\infty} v f(x, v, t)\, \mathrm{d}v\, \mathrm{d}x \tag{29}$$

$$W = \int_0^L \left[\int_{-\infty}^{\infty} \frac{v^2}{2} f(x, v, t)\, \mathrm{d}v + \frac{E^2(x, t)}{2} \right] \mathrm{d}x \tag{30}$$

which describe the conservation of the energy norm (S), the total number of electrons (N), total momentum (P) and total energy (W), respectively.

The corresponding invariants for the Fourier-transformed system (19)–(20) are:

$$S' = \int_0^L \int_{-\infty}^{\infty} |\hat{f}(x, \eta, t)|^2\, \mathrm{d}\eta\, \mathrm{d}x \tag{31}$$

$$N = \int_0^L 2\pi \hat{f}(x, 0, t)\, \mathrm{d}x \tag{32}$$

$$P = \int_0^L -\mathrm{i}2\pi \left[\frac{\partial \hat{f}(x, \eta, t)}{\partial \eta} \right]_{\eta = 0} \mathrm{d}x \tag{33}$$

$$W = \int_0^L \left\{ -\pi \left[\frac{\partial^2 \hat{f}(x, \eta, t)}{\partial \eta^2} \right]_{\eta = 0} + \frac{E^2(x, t)}{2} \right\} \mathrm{d}x \tag{34}$$

In the absence of an analytical "calibration" solution, it is important to check how well a numerical scheme conserves these invariants.

2.6. The Well-Posedness of the Continuous Problem

The equation system (19)–(20) is valid for all η on the real axis. In order to simulate numerically the system on an equidistant grid, one must however truncate the solution domain in the η direction, so that, for example, $-\eta_{\max} \leqslant \eta \leqslant \eta_{\max}$. Using the symmetry (25), this gives rise to boundaries at $\eta = 0$ and $\eta = \eta_{\max}$.

The boundary $\eta = \eta_{\max}$ must be treated with care so that it does not give rise to reflection of waves or to instabilities. One strategy is to let outgoing waves travel out over the boundary and to give a boundary condition equal to zero for incoming waves. This gives a mathematically well-posed problem.

In order to explore this idea one can study the initial value problem,

$$\frac{\partial \hat{f}}{\partial t} - \mathrm{i}\,\frac{\partial^2 \hat{f}}{\partial x\,\partial \eta} = 0 \tag{35}$$

$$f(x, \eta, 0) = f_0(x, \eta) \tag{36}$$

at the boundary $\eta = \eta_{\max}$. Fourier-transforming Eq. (35) in the x direction gives a new differential equation for the unknown function $\tilde{f}(k_x, \eta, t)$,

$$\frac{\partial \tilde{f}}{\partial t} + k_x \frac{\partial \tilde{f}}{\partial \eta} = 0 \tag{37}$$

$$\tilde{f}(k_x, \eta, 0) = \tilde{f}_0(k_x, \eta) \tag{38}$$

The general solution to this equation is

$$\tilde{f}(k_x, \eta, t) = \tilde{f}_0(\eta - k_x t) \tag{39}$$

for some arbitrary function $\tilde{f}_0$. It describes outgoing waves at $\eta = \eta_{\max}$ for $k_x > 0$ and incoming waves for $k_x < 0$.

Assuming the initial condition to be zero at the boundary $\eta = \eta_{\max}$ at the time $t = 0$, a well-posed boundary condition is

$$\begin{cases} \dfrac{\partial \tilde{f}}{\partial t} + k_x \dfrac{\partial \tilde{f}}{\partial \eta} = 0, & k_x > 0, \quad \eta = \eta_{\max} \\ \dfrac{\partial \tilde{f}}{\partial t} = 0, & k_x \leqslant 0, \quad \eta = \eta_{\max} \end{cases} \tag{40}$$

which can be expressed in terms of the Heaviside step function as

$$\frac{\partial \tilde{f}}{\partial t} + H(k_x)\, k_x \frac{\partial \tilde{f}}{\partial \eta} = 0, \qquad \eta = \eta_{\max} \tag{41}$$

where the Heaviside step function is defined as

$$H(k_x) = \begin{cases} 1, & k_x > 0 \\ 0, & k_x \leqslant 0 \end{cases} \tag{42}$$

The Heaviside function is commonly defined to take the value 1/2 for $k_x = 0$, but the function value at that point will not make any difference

in what follows. The boundary condition (40)–(41) allows outgoing waves to pass over the boundary and to be lost, while incoming waves are set to zero; the loss of the outgoing waves corresponds to the loss of the finest structures in velocity space.

Inverse Fourier transforming Eq. (41) then gives the boundary condition for the original problem (35) as

$$\frac{\partial \hat{f}}{\partial t} + \mathrm{F}^{-1} H(k_x)\, \mathrm{F}\left(-\mathrm{i}\, \frac{\partial^2 \hat{f}}{\partial x\, \partial \eta} \right) = 0, \qquad \eta = \eta_{\max} \tag{43}$$

where the spatial Fourier transform and inverse spatial Fourier transform is defined as

$$\mathrm{F}\phi = \int_{-\infty}^{\infty} \phi(x)\, e^{-\mathrm{i}k_x x}\, \mathrm{d}x \tag{44}$$

and

$$\mathrm{F}^{-1}\tilde{\phi} = \frac{1}{2\pi} \int_{-\infty}^{\infty} \tilde{\phi}(k_x)\, e^{\mathrm{i}k_x x}\, \mathrm{d}k_x \tag{45}$$

respectively. The projection operator $\mathrm{F}^{-1}H(k_x)\,\mathrm{F}$ projects a function onto the space of functions with only positive Fourier components in the x direction.

Problem (19) is treated according to the same idea,

$$\frac{\partial \hat{f}}{\partial t} + \mathrm{F}^{-1} H(k_x)\, \mathrm{F}\left(-\mathrm{i}\, \frac{\partial^2 \hat{f}}{\partial x\, \partial \eta} + \mathrm{i}\eta E \hat{f} \right) = 0, \qquad \eta = \eta_{\max} \tag{46}$$

which prevents the $\mathrm{i}\eta E\hat{f}$ term from producing spurious waves at the boundary.

The continuous problem is well-posed if the energy norm

$$\|\hat{f}\|^2 = \int_{x=0}^{L} \int_{\eta=0}^{\eta_{\max}} |\hat{f}|^2\, \mathrm{d}\eta\, \mathrm{d}x = \int_{x=0}^{L} \int_{\eta=0}^{\eta_{\max}} \hat{f}\hat{f}^*\, \mathrm{d}\eta\, \mathrm{d}x \tag{47}$$

of the solution is bounded for all times. In the following, we prove that this norm is monotonically decreasing with time. Taking the time derivative of the norm gives

$$\frac{\mathrm{d}\, \|\hat{f}\|^2}{\mathrm{d}t} = \int_{x=0}^{L} \int_{\eta=0}^{\eta_{\max}} \left(\hat{f}^* \frac{\partial \hat{f}}{\partial t} + \hat{f} \frac{\partial \hat{f}^*}{\partial t} \right) \mathrm{d}\eta\, \mathrm{d}x \tag{48}$$

and then replacing the time derivatives with the differential equation (19) gives

$$\begin{aligned}\frac{\mathrm{d}\,\|\hat{f}\|^2}{\mathrm{d}t} &= \int_{x=0}^{L}\int_{\eta=0}^{\eta_{\max}}\left[\hat{f}^*\left(\mathrm{i}\,\frac{\partial^2\hat{f}}{\partial x\,\partial\eta}-\mathrm{i}\eta E\hat{f}\right)+\hat{f}\left(-\mathrm{i}\,\frac{\partial^2\hat{f}^*}{\partial x\,\partial\eta}+\mathrm{i}\eta E\hat{f}^*\right)\right]\mathrm{d}\eta\,\mathrm{d}x\\ &= \int_{x=0}^{L}\int_{\eta=0}^{\eta_{\max}}\left[\mathrm{i}\left(\hat{f}^*\frac{\partial^2\hat{f}}{\partial x\,\partial\eta}-\hat{f}\,\frac{\partial^2\hat{f}^*}{\partial x\,\partial\eta}\right)-\mathrm{i}\hat{f}\hat{f}^*\,\eta\underbrace{(E-E^*)}_{=0,\,(E\text{ real})}\right]\mathrm{d}\eta\,\mathrm{d}x\\ &= \mathrm{i}\int_{x=0}^{L}\int_{\eta=0}^{\eta_{\max}}\left[\frac{\partial}{\partial\eta}\left(\hat{f}^*\frac{\partial\hat{f}}{\partial x}\right)-\frac{\partial}{\partial x}\left(f\,\frac{\partial f^*}{\partial\eta}\right)\right]\mathrm{d}\eta\,\mathrm{d}x\\ &= \mathrm{i}\int_{x=0}^{L}\left[\hat{f}^*\frac{\partial\hat{f}}{\partial x}\right]_{\eta=0}^{\eta_{\max}}\mathrm{d}x-\mathrm{i}\int_{\eta=0}^{\eta_{\max}}\left[\hat{f}\,\frac{\partial f^*}{\partial\eta}\right]_{x=0}^{L}\mathrm{d}\eta \qquad (49)\end{aligned}$$

where the second term vanishes due to periodic boundary conditions in the x direction, giving

$$\begin{aligned}\frac{\mathrm{d}\,\|\hat{f}\|^2}{\mathrm{d}t} &= \mathrm{i}\int_{x=0}^{L}\left[\hat{f}^*\frac{\partial\hat{f}}{\partial x}\right]_{\eta=0}^{\eta_{\max}}\mathrm{d}x\\ &= \mathrm{i}\int_{x=0}^{L}\hat{f}^*(x,\eta_{\max},t)\,\frac{\partial\hat{f}}{\partial x}(x,\eta_{\max},t)\,\mathrm{d}x\\ &\quad -\mathrm{i}\int_{x=0}^{L}\hat{f}^*(x,0,t)\,\frac{\partial\hat{f}}{\partial x}(x,0,t)\,\mathrm{d}x \qquad (50)\end{aligned}$$

The second term in (50) vanishes because, due to the symmetry (25), the imaginary part of the function is zero along the boundary $\eta=0$. This yields

$$\begin{aligned}-\mathrm{i}\int_{x=0}^{L}\hat{f}^*(x,0,t)\,\frac{\partial\hat{f}}{\partial x}(x,0,t)\,\mathrm{d}x &= -\mathrm{i}\int_{x=0}^{L}\hat{f}^{(\Re)}(x,0,t)\,\frac{\partial\hat{f}^{(\Re)}}{\partial x}(x,0,t)\,\mathrm{d}x\\ &= -\mathrm{i}\left[\frac{1}{2}\,\hat{f}^{(\Re)}(x,0,t)^2\right]_{x=0}^{L}=0 \qquad (51)\end{aligned}$$

What remains is

$$\frac{\mathrm{d}\,\|\hat{f}\|^2}{\mathrm{d}t}=\mathrm{i}\int_{x=0}^{L}\hat{f}^*(x,\eta_{\max},t)\,\frac{\partial\hat{f}}{\partial x}(x,\eta_{\max},t)\,\mathrm{d}x \qquad (52)$$

Along the boundary $\eta = \eta_{\max}$, the boundary condition (46) is applied. This equation can formally be integrated with respect to time, which gives

$$\begin{aligned}
&\hat{f}(x, \eta_{\max}, t) \\
&\quad = \int_{t'=0}^{t} \mathrm{F}^{-1} H(k_x)\, \mathrm{F} \left[\mathrm{i} \frac{\partial^2 \hat{f}}{\partial x\, \partial \eta}(x, \eta_{\max}, t') - \mathrm{i}\eta E(x, t')\, \hat{f}(x, \eta_{\max}, t') \right] \mathrm{d}t' \\
&\quad = \mathrm{F}^{-1} H(k_x)\, \mathrm{F} \int_{t'=0}^{t} \left[\mathrm{i} \frac{\partial^2 \hat{f}}{\partial x\, \partial \eta}(x, \eta_{\max}, t') - \mathrm{i}\eta E(x, t')\, \hat{f}(x, \eta_{\max}, t') \right] \mathrm{d}t' \\
&\quad = \mathrm{F}^{-1} H(k_x)\, \mathrm{F}\, g(x, t)
\end{aligned} \tag{53}$$

where

$$g(x, t) = \int_{t'=0}^{t} \left[\mathrm{i} \frac{\partial^2 \hat{f}}{\partial x\, \partial \eta}(x, \eta_{\max}, t') - \mathrm{i}\eta E(x, t')\, \hat{f}(x, \eta_{\max}, t') \right] \mathrm{d}t' \tag{54}$$

The expression (53) inserted into (52) gives

$$\frac{\mathrm{d}\, \|\hat{f}\|^2}{\mathrm{d}t} = \mathrm{i} \int_{x=0}^{L} [\mathrm{F}^{-1} H(k_x)\, \mathrm{F}\, g(x, t)]^* \frac{\partial}{\partial x} [\mathrm{F}^{-1} H(k_x)\, \mathrm{F}\, g(x, t)]\, \mathrm{d}x \tag{55}$$

Due to periodic boundary conditions in the x direction, the function g can be expanded into a Fourier series,

$$g(x, t) = \sum_{\omega=-\infty}^{\infty} \hat{g}_\omega(t)\, e^{\mathrm{i}2\pi\omega(x/L)} \tag{56}$$

Taking the Fourier transform of this expression gives

$$\begin{aligned}
\mathrm{F}\, g(x, t) &= \int_{-\infty}^{\infty} e^{-\mathrm{i}k_x x} \sum_{\omega=-\infty}^{\infty} \hat{g}_\omega(t)\, e^{\mathrm{i}2\pi\omega(x/L)}\, \mathrm{d}x \\
&= \sum_{\omega=-\infty}^{\infty} \hat{g}_\omega(t) \int_{-\infty}^{\infty} e^{\mathrm{i}((2\pi\omega/L) - k_x) x}\, \mathrm{d}x \\
&= \sum_{\omega=-\infty}^{\infty} \hat{g}_\omega(t)\, 2\pi\delta_0 \left(\frac{2\pi\omega}{L} - k_x \right)
\end{aligned} \tag{57}$$

where δ_0 is the Dirac delta measure.

Multiplying this expression by the Heaviside function truncates the infinite sum as

$$H(k_x)\,\mathrm{F}g(x,t) = \sum_{\omega=-\infty}^{\infty} \hat{g}_\omega(t)\,2\pi H(k_x)\,\delta_0\left(\frac{2\pi\omega}{L}-k_x\right)$$
$$= \sum_{\omega=1}^{\infty} \hat{g}_\omega(t)\,2\pi\delta_0\left(\frac{2\pi\omega}{L}-k_x\right) \tag{58}$$

since $\omega \leqslant 0$ gives zero contribution to the sum.

Inverse Fourier transforming expression 58 gives

$$\mathrm{F}^{-1}H(k_x)\,\mathrm{F}g(x,t) = \frac{1}{2\pi}\int_{-\infty}^{\infty} [H(k_x)\,\mathrm{F}g(x,t)]\,e^{\mathrm{i}k_x x}\,\mathrm{d}k_x$$
$$= \sum_{\omega=1}^{\infty} \hat{g}_\omega(t)\int_{-\infty}^{\infty} \delta_0\left(\frac{2\pi\omega}{L}-k_x\right) e^{\mathrm{i}k_x x}\,\mathrm{d}k_x$$
$$= \sum_{\omega=1}^{\infty} \hat{g}_\omega(t)\,e^{\mathrm{i}(2\pi\omega/L)\,x} \tag{59}$$

which, inserted into (55), gives

$$\frac{\mathrm{d}\,\|\hat{f}\|^2}{\mathrm{d}t} = \mathrm{i}\int_{x=0}^{L}\left[\sum_{\omega=1}^{\infty} \hat{g}_\omega(t)\,e^{\mathrm{i}(2\pi\omega/L)\,x}\right]^* \frac{\partial}{\partial x}\left[\sum_{\omega=1}^{\infty} \hat{g}_\omega(t)\,e^{\mathrm{i}(2\pi\omega/L)\,x}\right]\mathrm{d}x$$
$$= \mathrm{i}\int_{x=0}^{L}\left[\sum_{\omega=1}^{\infty} \hat{g}_\omega^*(t)\,e^{-\mathrm{i}(2\pi\omega/L)\,x}\right]\left[\sum_{\omega=1}^{\infty} \hat{g}_\omega(t)\,\mathrm{i}\,\frac{2\pi\omega}{L}\,e^{\mathrm{i}(2\pi\omega/L)\,x}\right]\mathrm{d}x$$
$$= -\frac{2\pi}{L}\int_{x=0}^{L}\sum_{\omega=1}^{\infty} \hat{g}_\omega^*(t)\,\hat{g}_\omega(t)\,\omega\,\mathrm{d}x = -2\pi\sum_{\omega=1}^{\infty} |\hat{g}_\omega(t)|^2\,\omega \leqslant 0 \tag{60}$$

Thus we have proved that the energy norm is non-increasing with time, and therefore the continuous problem wit the given boundary conditions is well-posed.

3. THE NUMERICAL APPROACH

3.1. Storage of the Solution

This section discusses the number of grid points and the amount of data needed for storing the solution.

When storing the distribution function $f(x, v, t)$ on a grid there are two problems to keep in mind.

1. The function is defined for all velocities, but numerically one has to truncate the solution domain at some "high" velocity $v_{\max}$, where the function values have become small enough.
2. The function may contain fine structures in the v direction, and one has to have a fine enough grid to represent these fine structures.

These two problems have their counterparts in the inverse Fourier transformed variables; a less localised function in v space leads to finer structures in the η space, and finer structures in v space leads to a less localised function in η space. To be precise, the two problems are converted to

1. Assuming that the maximum velocity for particles is $v = v_{\max}$, then after Fourier transforming the function $f(x, v, t)$, the quantity $k_{\eta,\max} = v_{\max}$ will be the maximum wave number in the η direction, and the minimum "wavelength" will then be $\lambda_{\eta,\min} = 2\pi/k_{\eta,\max} = 2\pi/v_{\max}$. According to the Nyqvist sampling theorem one needs at least two grid points per wavelength to represent the solution, so the condition on the grid size becomes $\Delta\eta < \lambda_{\eta,\min}/2 = \pi/v_{\max}$.
2. Assuming that the shortest "wavelength" to be resolved in the v direction is $\lambda_{v,\min}$, the highest wave number in the v direction becomes $k_{v,\max} = 2\pi/\lambda_{v,\min}$. After Fourier transformation, this gives a condition on the domain size in the η direction as $\eta_{\max} \geqslant k_{v,\max} = 2\pi/\lambda_{v,\min}$.

The number of grid points needed to store the function $f(x, \eta, t)$ on the interval $0 \leqslant \eta \leqslant \eta_{\max}$ [for negative η one can use symmetry relation (25)] is then

$$N_\eta = \frac{\eta_{\max}}{\Delta\eta} > 2\frac{v_{\max}}{\lambda_{v,\min}} \tag{61}$$

For storing the original function $f(x, v, t)$ one needs to store the function one the domain $-v_{\max} \leqslant v \leqslant v_{\max}$, with the grid size $\Delta v < \lambda_{v,\min}/2$ according to the sampling theorem. This gives the number of grid points in the v direction as

$$N_v = \frac{2v_{\max}}{\Delta v} > 4\frac{v_{\max}}{\lambda_{v,\min}} \tag{62}$$

Thus one needs twice as many grid points to store the original function $f(x, v, t)$ compared to storing the Fourier transformed function $\hat{f}(x, \eta, t)$. However, the function $\hat{f}(x, \eta, t)$ is complex valued so the *amount of data* to store is the same for $\hat{f}(x, \eta, t)$ as for $f(x, v, t)$.

3.2. Discretization

We discretize the problem on a rectangular, equidistant grid with periodic boundary conditions in the x direction. In the η direction the grid starts at $\eta = 0$ and ends at some positive $\eta = \eta_{\max}$.

The approximate function values at the grid points are enumerated such that

$$\hat{f}(x_i, \eta_j, t_k) \approx \hat{f}^k_{i,j} \tag{63}$$

with

$$x_i = i\,\Delta x, \qquad i = 0, 1, \ldots, N_x - 1 \tag{64}$$

$$\eta_j = j\,\Delta\eta, \qquad j = 0, 1, \ldots, N_\eta \tag{65}$$

$$t_k = k\,\Delta t, \qquad k = 0, 1, \ldots, N_t \tag{66}$$

where

$$\Delta x = \frac{L}{N_x} \tag{67}$$

$$\Delta\eta = \frac{\eta_{\max}}{N_\eta} \tag{68}$$

$$\Delta t = \frac{t_{\text{end}}}{N_t} \tag{69}$$

3.3. Numerical Approximations

The Vlasov–Poisson system (19, 20) together with the boundary condition (46) at $\eta = \eta_{\max}$ is approximated by a semi-discretization in x and η space. After that, time steps are taken with the fourth-order Runge–Kutta method.

In order to see the semi-discretization, the equations are rewritten on the form

$$\frac{\partial \hat{f}}{\partial t} = \mathrm{i}\,\frac{\partial^2 \hat{f}}{\partial x\,\partial \eta} - \mathrm{i}\eta E\hat{f}, \qquad 0 \leqslant \eta < \eta_{\max}, \quad 0 \leqslant x < L \tag{70}$$

$$\frac{\partial E(x,t)}{\partial x} = 1 - 2\pi \hat{f}(x,0,t) \tag{71}$$

$$\frac{\partial \hat{f}}{\partial t} = \mathrm{F}^{-1} H(k_x)\,\mathrm{F}\left(\mathrm{i}\,\frac{\partial^2 \hat{f}}{\partial x\,\partial \eta} - \mathrm{i}\eta E\hat{f}\right), \qquad \eta = \eta_{\max}, \quad 0 \leqslant x < L \tag{72}$$

$$\hat{f}(L,\eta,t) = \hat{f}(0,\eta,t) \tag{73}$$

Equation (71) is solved numerically to obtain E, which is then used to calculate the right-hand sides in Eqs. (70) and (72); one can see E as a *function* of f. The η and x derivatives in Eqs. (70) and (72) are calculated numerically, as well as the operator $\mathrm{F}^{-1}H(k_x)\,\mathrm{F}$ in Eq. (72); the methods will be described below. By these approximations and after discretizations in x and η directions according to the previous section, the equation is approximated by the semi-discretization

$$\frac{\partial \hat{f}_{i,j}}{\partial t} = P(\hat{f})_{i,j} \tag{74}$$

where P is a grid function representing the numerical approximation of the right-hand sides of Eqs. (70) and (72); the function P is a function of all $\hat{f}_{i,j}$. The unknown $\hat{f}_{i,j}$ is then discretized also in *time*, and the time-stepping is done with the well-known Runge–Kutta algorithm:

1. $F^{(1)}_{i,j} \leftarrow P(\hat{f}^k),\ \forall i, j$
2. $F^{(2)}_{i,j} \leftarrow P(\hat{f}^k + F^{(1)}\Delta t/2),\ \forall i, j$
3. $F^{(3)}_{i,j} \leftarrow P(\hat{f}^k + F^{(2)}\Delta t/2),\ \forall i, j$
4. $F^{(4)}_{i,j} \leftarrow P(\hat{f}^k + F^{(3)}\Delta t),\ \forall i, j$
5. $\hat{f}^{k+1}_{i,j} \leftarrow \hat{f}^k_{i,j} + (\Delta t/6)(F^{(1)}_{i,j} + 2F^{(2)}_{i,j} + 2F^{(3)}_{i,j} + F^{(4)}_{i,j}),\ \forall i, j$

The steps needed for obtaining the approximation $P_{i,j}$ are:

1. Calculate the electric field numerically from Eq. (71).
2. Calculate a numerical approximation of Eq. (70), for all points *including the points along the boundary* $\eta = \eta_{\max}$.
3. Apply numerically the boundary condition (72) for the points along the boundary $\eta = \eta_{\max}$.

The periodic boundary condition (73) eliminates in practice the boundary at $x = L$. There is no need to store the function value corresponding to $x = L$, and, when needed, one uses the rule $\hat{f}(x, \eta, t) = \hat{f}(x - L, \eta, t)$ for $x \geqslant L$, and the rule $\hat{f}(x, \eta, t) = \hat{f}(x + L, \eta, t)$ for $x < 0$. The corresponding rules for the discrete case are $\hat{f}_{i,j} = \hat{f}_{i-N_x,j}$ for $i \geqslant N_x$ and $\hat{f}_{i,j} = \hat{f}_{i+N_x,j}$ for $i < 0$, respectively.

Due to the periodicity in the x direction, a pseudo-spectral method can be used to calculate the x derivatives in the Eqs. (70)–(72) accurately. The Fourier transform and its inverse in approximated by the discrete Fourier transform and inverse discrete Fourier transform, respectively. The discrete transforms are efficiently calculated by using the *fast Fourier transform* (FFT) and *inverse fast Fourier transform* (*IFFT*) algorithms. Symbolically the notations $\mathrm{F} \approx \mathrm{FFT}$ and $\mathrm{F}^{-1} \approx \mathrm{IFFT}$ are used.

By using the well-known relation for the Fourier transform

$$\frac{\partial \phi}{\partial x} = \mathrm{F}^{-1}\mathrm{F}\frac{\partial \phi}{\partial x} = \mathrm{F}^{-1}\mathrm{i}k_x\,\mathrm{F}\phi \tag{75}$$

the corresponding approximation of the x derivative, used in the discretized case, is

$$\frac{\partial \phi}{\partial x} \approx \mathrm{IFFT}[\mathrm{i}k_x\,\mathrm{FFT}(\phi)] \tag{76}$$

The integration of E is approximated by

$$E \approx \mathrm{IFFT}\left[\frac{1}{\mathrm{i}k_x}\,\mathrm{FFT}(1 - 2\pi\hat{f}^k_{i,0})\right] \tag{77}$$

except for $k_x = 0$. The component corresponding to $k_x = 0$ is set equal to zero.

The numerical approximation of the x derivatives in Eqs. (70) and (72) with

$$\frac{\partial^2 \hat{f}}{\partial x\,\partial \eta} = \frac{\partial}{\partial \eta}\left(\frac{\partial \hat{f}}{\partial x}\right) \tag{78}$$

is performed as

$$\frac{\partial \hat{f}}{\partial x} \approx \mathrm{IFFT}[\mathrm{i}k_x\,\mathrm{FFT}(\hat{f}^k_{i,j})] \tag{79}$$

In the η direction, the derivative $v = \partial \hat{f}/\partial \eta$ is calculated using the classical fourth order Padé scheme [5, 6]. For the inner points, the implicit approximation

$$v_{i,j-1} + 4v_{i,j} + v_{i,j+1} = \frac{3}{\Delta\eta}(\hat{f}_{i,j+1} - \hat{f}_{i,j-1}), \qquad j = 1, 2, \ldots, N_\eta - 1 \tag{80}$$

is used. A family of similar schemes exists [6].

At the boundary $\eta = 0$, the symmetry (25) and (26) is used to apply the same approximation of the derivative at the boundary as for the inner points. The relations $\hat{f}_{i,-1} = \hat{f}^*_{i,1}$ and $v_{i,-1} = -v^*_{i,1}$ give

$$-v^*_{i,1} + 4v_{i,0} + v_{i,1} = \frac{3}{\Delta\eta}(\hat{f}_{i,1} - \hat{f}^*_{i,1}) \tag{81}$$

or, for the real and imaginary parts,

$$v^{(\Re)}_{i,0} = 0 \tag{82}$$

$$2v^{(\Im)}_{i,0} + v^{(\Im)}_{i,1} = \frac{3}{\Delta\eta}\hat{f}^{(\Im)}_{i,1} \tag{83}$$

respectively.

At the boundary $\eta = \eta_{\max}$, a one-sided approximation,

$$v_{i,N_\eta} + 2v_{i,N_\eta-1} = -\frac{1}{2\Delta\eta}(-5\hat{f}_{i,N_\eta} + 4\hat{f}_{i,N_\eta-1} + \hat{f}_{i,N_\eta-2}) \tag{84}$$

is used, which gives a truncation error of order $\Delta\eta^3$ at the boundary.

The Eqs. (80), (81) and (84) form one tridiagonal equation system for each subscript $i = 0, 1, \ldots, N_x$, each system having N_η complex-valued unknowns. In practice the equation system can be divided into systems for the real and imaginary parts separately.

At the boundary $\eta = \eta_{\max}$ the boundary condition (72) is applied, with the help of the approximation

$$\mathrm{F}^{-1}H(k_x)\,\mathrm{F}\phi(x, \eta_{\max}, t) \approx \mathrm{IFFT}[H(k_x)\,\mathrm{FFT}(\phi^k_{i,N_\eta})] \tag{85}$$

with $\phi(x, \eta_{\max}, t)$ being the right-hand side of (70) along the boundary $\eta = \eta_{\max}$ and ϕ^k_{i,N_η} its discrete approximation.

In order to reduce aliasing effects in the x direction, a sixth-order dissipative term is added to Eq. (19), which changes into

$$\frac{\partial \hat{f}}{\partial t} - \mathrm{i}\,\frac{\partial^2 \hat{f}}{\partial x\,\partial \eta} + \mathrm{i}\eta E\hat{f} - \delta(\Delta x)^4\,\frac{\partial^6 \hat{f}}{\partial x^6} = 0 \tag{86}$$

where the real constant δ is chosen to some small positive number. The sixth derivative is approximated with a centred second-order approximation.

3.4. Stability Analysis

When solving the reduced problem

$$\frac{\partial \hat{f}}{\partial t} - \mathrm{i}\,\frac{\partial^2 \hat{f}}{\partial x\,\partial \eta} = 0 \tag{87}$$

with an explicit scheme, the stability region is

$$\Delta t < \frac{\rho}{K_x K_\eta} \tag{88}$$

where $\rho = \sqrt{8}$ for the explicit Runge–Kutta scheme, and K_x and K_η are the maximum values of the approximations of wave numbers produced by the numerical scheme in x and η direction, respectively.

In the x direction the spectral method gives a maximum value of the approximated wave number equal to

$$K_x = \frac{\pi}{\Delta x} \tag{89}$$

In the η direction the Padé scheme, applied to a continuous function, is

$$v(\eta - \Delta\eta) + 4v(\eta) + v(\eta + \Delta\eta) = \frac{3}{\Delta\eta}\,[\hat{f}(\eta + \Delta\eta) - \hat{f}(\eta - \Delta\eta)] \tag{90}$$

which, with $v(\eta) = \tilde{v}\exp(\mathrm{i}k_\eta \eta)$ and $\hat{f}(\eta) = \tilde{f}\exp(\mathrm{i}k_\eta \eta)$, gives

$$\tilde{v} = \mathrm{i}\,\frac{3}{\Delta\eta}\,\frac{\sin(k_\eta\,\Delta\eta)}{[2 + \cos(k_\eta\,\Delta\eta)]}\,\tilde{f} \tag{91}$$

Hence, the maximum value of the approximated wavenumber in the η direction is

$$K_\eta = \max_{0 \leqslant k_\eta \Delta\eta \leqslant \pi} \left| \frac{3}{\Delta\eta} \frac{\sin(k_\eta \Delta\eta)}{[2 + \cos(k_\eta \Delta\eta)]} \right| = \frac{\sqrt{3}}{\Delta\eta} \tag{92}$$

where the maximum is obtained for $k_\eta \Delta\eta = 2\pi/3$.

Inserting the expressions for ρ, K_x and K_η into (88) then gives the choice of Δt as

$$\Delta t < \frac{\sqrt{8}}{\sqrt{3}\,\pi} \Delta x \, \Delta\eta \approx 0.52 \Delta x \, \Delta\eta \tag{93}$$

for stability at the inner points. Introducing the so-called *CFL number*, the condition (93) can be expressed as

$$\Delta t = CFL \frac{\sqrt{8}}{\sqrt{3}\,\pi} \Delta x \, \Delta\eta \tag{94}$$

where the positive number

$$CFL < 1 \tag{95}$$

for stability.

The nonlinearity and boundary conditions are not treated in this analysis. Some numerical tests have shown that $CFL = 0.8$ gives stability while $CFL = 0.9$ gives instability; see also Section 4.

3.5. The Conservation of Particles

It is easily shown that the numerical scheme conserves exactly the total number of particles (32), approximated by the formula

$$N = 2\pi \sum_{i=0}^{N_x - 1} \hat{f}^k_{i,0} \Delta x \tag{96}$$

The sum only picks up the zeroth Fourier component of $\hat{f}^k_{i,0}$, corresponding to $k_x = 0$, and that component is left unchanged since it vanishes in the term containing the x derivative in Eq. (19) with the approximation (79). Along the boundary $\eta = 0$ the last term in (19) also vanishes. This result has been verified in the numerical experiments where the number of particles are conserved by the numerical scheme up to the precision of the computer.

4. NUMERICAL RESULTS

4.1. Reflections Off Boundaries

In order to verify that waves are absorbed by the boundary at $\eta = \eta_{\max}$, and that thereby the recurrence phenomenon is reduces, a numerical experiment was carried out. The simulation domain was chosen to be $0 \leqslant x \leqslant 4\pi$, $0 \leqslant \eta \leqslant 20$. The number of grid points in the x direction was $N_x = 100$. The initial condition was chosen according to Eq. (102) below with the amplitude $A = 0.0002$ and the wavenumber $k_x = 0.5$; this choice assured that the wave was linearly damped according to known theory [11]. Three numerical experiments can be seen in Fig. 1, which shows the time development of the first spatial harmonic of the electric field. Curve (a) shows a simulation with the outgoing wave boundary condition and with the grid size $\Delta\eta = 2/15$, and in curve (b) the grid has been made coarser, $\Delta\eta = 2/10$. As a reference, curve (c) shows a simulation with the commonly used [1, 3] Dirichlet-type of boundary condition $\hat{f}(x, \eta_{\max}, t) = 0$ on the finer grid $\Delta\eta = 2/15$.

As can be seen in Fig. 1, the solutions are initially exponentially damped, and at about $t = 50$ one can see some smaller reflections from the boundary,

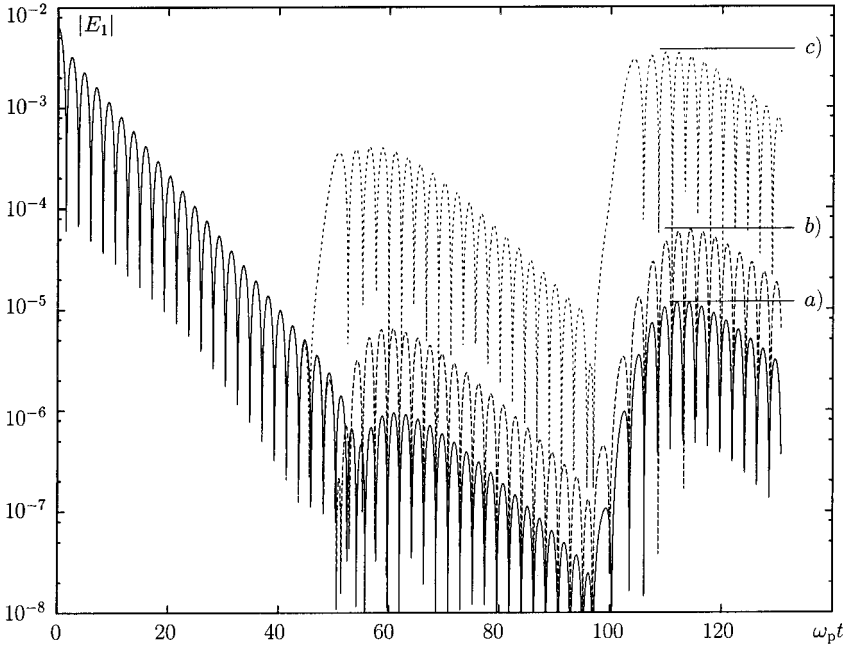

Fig. 1. Reflections of waves against the boundary $\eta = \eta_{\max}$.

followed by a much stronger reflection at $t = 100$. The solution on the finest grid (a) with outgoing wave boundary conditions shows a reflected wave with the amplitude about 1/1000 of the amplitude of the initial condition at $t = 0$, while the solution on the somewhat coarser grid (b) shows a reflected wave with the amplitude somewhat more than 1/100 of the initial amplitude. With the Dirichlet-type boundary condition (c), the reflected wave is of the same order in amplitude as the initial amplitude.

It is apparent from this numerical investigation that the outgoing wave boundary condition prevents, to a large extent, waves from returning back and ruining the calculations, while the simple Dirichlet-type boundary condition leads to an almost total reflection of waves. These reflected waves lead to a similar detrimental effect as the recurrence phenomenon in real velocity space.

4.2. Nonlinear Landau Damping

In order to ascertain that the numerical scheme reproduces some known non-linear effects, tests with larger initial amplitudes of the waves were carried out.

A simulation was performed with the initial condition according to, in terms of the original (x, v) variables,

$$f(x, v, 0) = (1 + A \cos(k_x x))\, f_0(x, v) \tag{97}$$

where f_0 was chosen as

$$f_0(x, v) = (2\pi)^{-1/2} \exp\left\{ -\frac{1}{2}\left[v - \frac{\omega}{k_x} A \cos(k_x x) \right]^2 \right\} \tag{98}$$

This is an approximation of a sinusoidal wave moving in the rightward direction. The approximate dispersion relation for Langmuir waves yields $\omega = \sqrt{1 + 3k_x^2}$. In the inverse Fourier transformed variables, the initial condition is converted into

$$\hat{f}(x, \eta, 0) = [\,1 + A \cos(k_x x)\,]\, \hat{f}_0(x, \eta) \tag{99}$$

where

$$\hat{f}_0(x, \eta) = \frac{1}{2\pi} \exp\left[\mathrm{i} \frac{\omega}{k_x} A \cos(k_x x)\, \eta \right] \exp\left(-\frac{1}{2}\eta^2 \right) \tag{100}$$

which is the initial condition used in the simulation.

The wave number $k_x = 0.25$ and amplitude $A = 0.15$ were chosen. The simulation domain was set to $0 \leqslant x \leqslant 24\pi$, $0 \leqslant \eta \leqslant 30$ with $N_x = 300$, $N_\eta = 150$

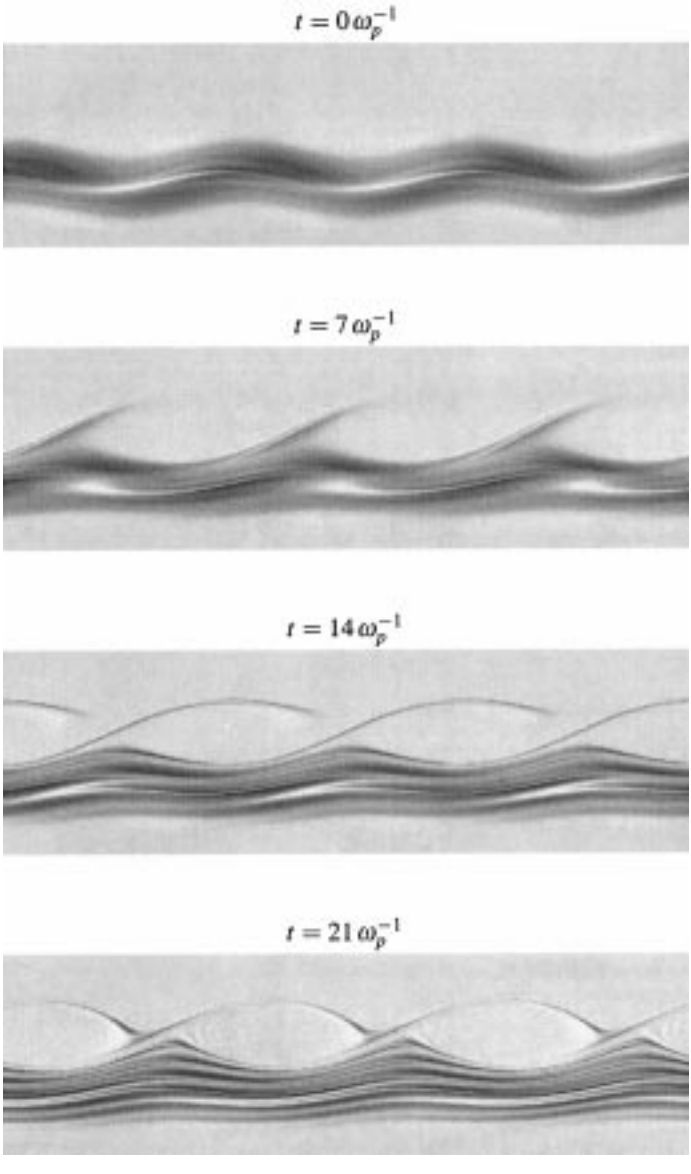

Fig. 2. The development of an electrostatic wave in phase space (x, v) at four different times. One can see particles getting trapped in the potential wells of the wave.

and $\Delta t = 0.00875$ ($CFL \approx 0.33$). The numerical dissipation was set to $\delta = 0.002$. In order to visualise the solution, it was Fourier transformed back to the real-valued function $f(x, v, t)$ and plotted in Fig. 2. One can see the process of electrons getting trapped and starting to oscillate in the potential wells of the wave. As expected, the solution becomes more and more structured due to the ballistic terms.

Another numerical experiment on nonlinear Landau damping was carried out, with the initial condition chosen to

$$f(x, v, 0) = [1 + A \cos(k_x x)]\, f_0(v) \tag{101}$$

where $A = 0.5$, $k_x = 0.5$ and $f_0(v) = (2\pi)^{-1/2} \exp(-v^2/2)$; this is identical to one of the experiments carried out by Cheng and Knorr [2].

In the inverse Fourier transformed variables the initial condition becomes

$$\hat{f}(x, \eta, 0) = [1 + A \cos(k_x x)]\, \hat{f}_0(\eta) \tag{102}$$

with $\hat{f}_0(\eta) = (2\pi)^{-1} \exp(-\eta^2/2)$. The simulation domain was chosen as $0 \leqslant x \leqslant 4\pi$ and $0 \leqslant \eta \leqslant 30$ with $N_x = N_\eta = 100$, and the time domain was chosen as $0 \leqslant t \leqslant 70$ with $N_t = 5000$ ($CFL \approx 0.71$). The numerical dissipation was set to $\delta = 0.001$. The amplitudes of the first three spatial components of the electric field were plotted against time in Fig. 3. One can

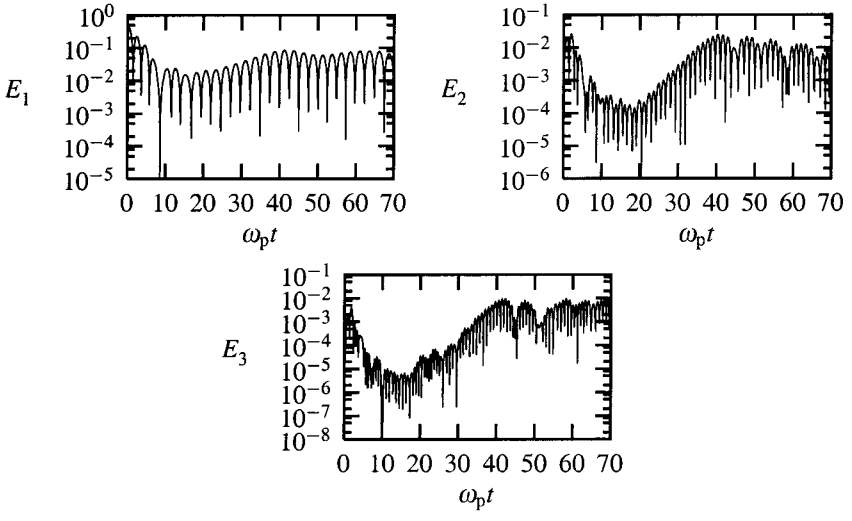

Fig. 3. The first three spatial harmonics of the electric field.

note a strong exponential damping of the amplitudes from $t=0$ to $t\approx 10$, in agreement with linear Landau theory. From $t\approx 20$ to $t\approx 40$ the modes grow exponentially, whereafter they oscillate around equilibria as the Landau damping enters the nonlinear regime [11]. These results are in excellent agreement with those obtained by Cheng and Knorr. These authors have made a deeper analysis of the results [2].

In order to test the long-term properties of our numerical method, a longer simulation was performed where the time domain was changed to $0\leqslant t\leqslant 7000$ and $N_t=500,000$, and the other parameters were kept unchanged.

No numerical instability could be detected in the simulation. The squared energy norm (47) was numerically approximated by using a sum representation of the double integral and its value, relative to its initial value, was plotted against the time in Fig. 4. Initially it decreases from unity down to an equilibrium state at about 0.8130 after which it exhibits very small fluctuations.

The time development of the total energy (34) is shown in Fig. 5. As can be see, the energy is almost entirely conserved. In order to calculate the second derivative in the formula for the energy, a centred sixth-order scheme was used together with the symmetry (25).

The behaviour of the first spatial mode of the electric field is shown in Fig. 6. The electric field is initially damped from the value 0.5 down to somewhat below 0.05 where the damping almost stops. In a numerical

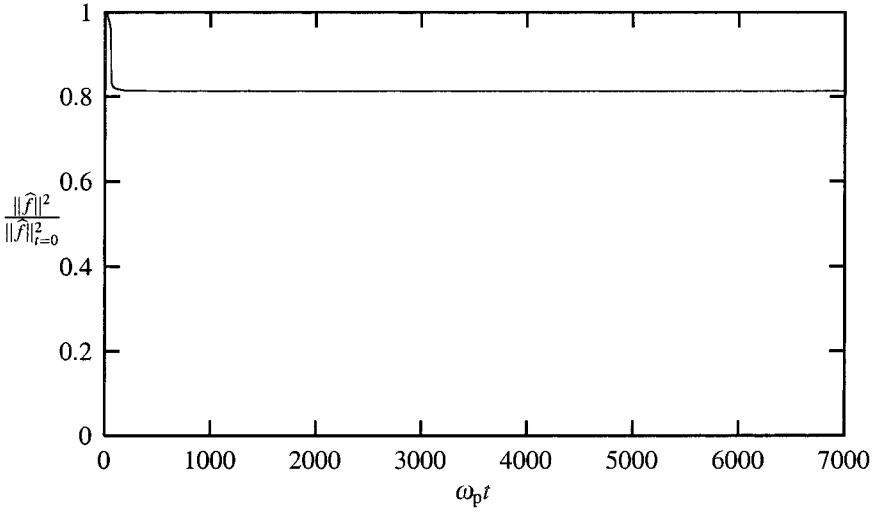

Fig. 4. The relative change for the squared norm.

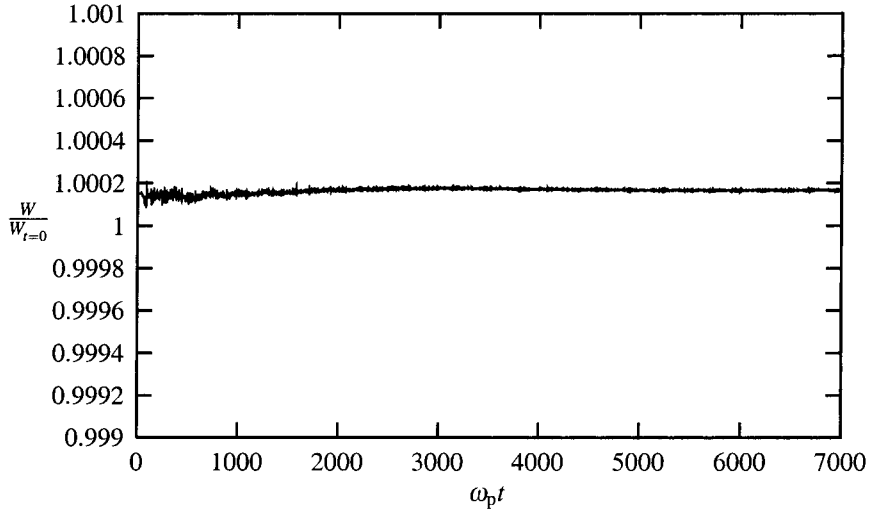

Fig. 5. The relative change of the total energy.

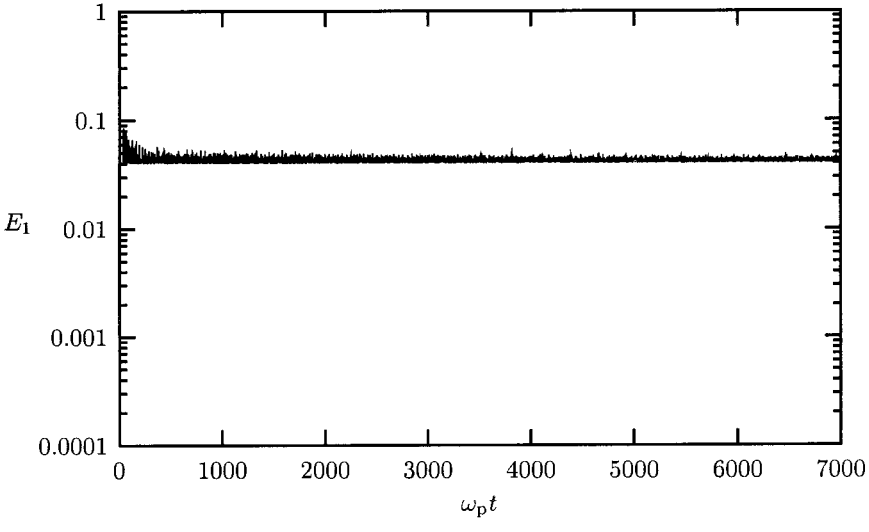

Fig. 6. The long-term behaviour of the amplitude of the first spatial mode of the electric field (Function value below 0.04 have been removed).

long-time experiment carried out by Manfredi [8], this general behavior of the solution could also be observed, for an almost similar problem.

5. CONCLUSIONS

A high-order method for solving numerically the Fourier transformed Vlasov–Poisson system in the velocity space has been studied, with a special attention paid to the outflow boundary condition in the Fourier transformed space. It was shown numerically that it is possible to reduce the recurrence phenomenon by this method.

The boundary condition designed for the transformed system has been proved to be well-posed in the continuous case. The numerical scheme did not exhibit any instabilities in the numerical experiments.

Our numerical scheme conserves the total number of particles of the system exactly and it conserves the total energy of the system to a very high degree.

Whether or not the method described in this article is better than existing methods will probably depend on the physical problem. Numerical tests are needed to determine in which cases our method may be a good alternative to existing methods.

ACKNOWLEDGMENTS

I want to thank professor Bertil Gustafsson at Department of Scientific Computing, Uppsala University, and professor Bo Thidé at Swedish Institute of Space Physics, Uppsala Division, for fruitful discussions and their useful advise during my work.

Special thanks to professor Helmut Neunzert at the university of Kaiserslauten, Germany, who kindly sent me published and unpublished material on the Boltzmann equation from his research.

This research was financially supported by the Swedish National Graduate School in Scientific Computing (NGSSC) and the Swedish National Sciences Research Council (NFR).

REFERENCES

1. Armstrong, T. P., Harding, R. C., Knorr, G., and Montgomery, D. (1970). Solution of Vlasov's equation by transform methods, *Methods in Computational Physics (Academic Press)* **9**, 29–86.
2. Cheng, C. Z., and Knorr, G. (1976). The integration of the Vlasov equation in configuration space, *J. Comput. Phys.* **22**, 330–351.

3. Denavit, J., and Kruer, W. L. (1971). Comparison of numerical solutions of the Vlasov equation with particle simulations of collisionless plasmas, *The Physics of Fluids*, 1782–1791.
4. Feng, J., and Hitchon, W. N. G. (1999). Self-consistent kinetic simulation of plasmas, *Phys. Rev. E* **61**, 3160–3173.
5. Gustafsson, B., and Olsson, P. (1995). Fourth-order difference methods for hyperbolic ibvps, *J. Comput. Phys.* **117**, 300–317.
6. Lele, S. K. (1992). Compact finite difference schemes with spectral-like resolution, *J. Comput. Phys.* **103**, 16–42.
7. Lin, Ching-Huei., Chao, J. K., and Cheng, C. Z. (1995). One-dimensional Vlasov simulations of Langmuir solitions, *Phys. Plasmas* **2**, 4195–4203.
8. Manfredi, G. (1997). Long-time behaviour of nonlinear Landau damping, *Phys. Rev. Lett.* **79**, 2815–2818.
9. Neunzert, H. (1981). An introduction to the nonlinear Boltzmann-Vlasov equation. Preprint No. 28. Lectures given at the international summerschool "Kinetic Theories and Boltzmann Equations" of C.I.M.E. in Montecatini (Italy).
10. Neunzert, H. (1971). Verallgemeinerte Lösungen von Eigenwertproblemen, zugehörige Entwicklungsfragen und die Anwendung auf Gleichungen der Transporttheorie, Jül-816-MA.
11. Schmidt, G. (1979). *Physics of High Temperature Plasmas*, 2nd ed., Academic Press, Inc., pp. 269–282.